Available online at www.sciencedirect.com

ScienceDirect

Procedia Structural Integrity 2 (2016) 3407–3414

Structural Integrity Procedia

www.elsevier.com/locate/procedia

21st European Conference on Fracture, ECF21, 20-24 June 2016, Catania, Italy

# Damage Evolution in Thermomechanical Loading of Stainless Steel

R. Petráš[a,b], V. Škorík[b], J. Polák[a,b]*

[a] *CEITEC IPM, Institute of Physics of Materials ASCR, Žižkova 22, 616 62 Brno, Czech Republic*
[b] *Institute of Physics of Materials ASCR, Žižkova 22, 616 62 Brno, Czech Republic*

**Abstract**

Superaustenitic stainless steel Sanicro 25 has been subjected to in-phase and out-of-phase thermomechanical fatigue (TMF). Different amplitudes of mechanical strain and the changes of the temperature in the interval 250 to 700°C were applied to standard cylindrical specimens. Early fatigue damage has been studied using scanning electron microscopy combined with FIB cutting and EBSD imaging. TMF loading resulted first in developing thin oxide layer. In in-phase loading grain boundaries were preferentially oxidized and fatigue cracks developed by alternating oxidation and cracking. Fatigue cracks developed rapidly in oxidized grain boundaries and propagated intergranularly. During out-of-phase TMF loading the cracked oxide layer resulted in local oxidation and crack initiation. The crack grew transgranularly.



*Keywords:* Thermomechanical fatigue; Sanicro 25 steel; Damage mechanism; FIB cutting; Localized oxidation-cracking

## 1. Introduction

Electrical energy is currently the most widely used type of energy around the world. Coal has a dominant role in worldwide electricity generation, Reddy (2013). Design and construction of novel, more efficient installations requires the usage of materials resisting severe loading and environmental conditions. Thermal and mechanical stresses in components during service produce variable strains and result in initiation and propagation of fatigue cracks. Low cycle fatigue, thermomechanical fatigue, creep-fatigue interaction, creep rupture strength under environmental conditions have to be considered in order to determine the rate of damage in materials working at elevated temperatures.

* Corresponding author. Tel.: +420 532 290 366;
*E-mail address:* polak@ipm.cz (J. Polák)


10.1016/j.prostr.2016.06.425

Austenitic stainless steel grade UNS S31035, Sandvik Sanicro 25, has been developed for the super-heaters and reheaters in future high-efficient coal fired boilers, Chai et al. (2013). It shows very good resistance to steam oxidation; hot corrosion and high creep rupture strength higher than the other austenitic steels.

Austenitic steels are widely used materials designated for high temperature applications. Several papers have been presented on thermomechanical fatigue (TMF) behavior and damage mechanism of individual types of stainless steel (SS), e.g. 304 SS, Kuwabara and Nitta (1976, 1979). The classification of the TMF life behavior according to the effect of fatigue, creep and environment on the lifetime was proposed by Nitta and Kuwabara (1988). Zauter et al. (1994) investigated the TMF behavior on 304L SS in vacuum. They reported that the TMF fatigue life and damage development was governed by maximum temperature of cycling. The differences between IP and OP-TMF fatigue lives of 316L SS in various temperature ranges were discussed by Shi et al. (1996). Hormozi et al. (2015) presented a detailed experimental study on failure of 316 SS material under IP-TMF and LCF loading conditions. The damage mechanism of advanced heat resistant Sanicro 25 in isothermal and TMF cycling was recently reported by Polák et al. (2014) and Petráš et al. (2016).

## 2. Experimental

### *2.1. Material*

Material employed for this study was austenitic heat resistant stainless steel Sanicro 25 provided by Sandvik, Sweden in the form of cylindrical rod of 150 mm in diameter. The chemical composition of the material can be found elsewhere, Polák et al. (2014).

Cylindrical specimens with gauge length 16 or 15 mm and a diameter 7 or 6 mm for thermomechanical and isothermal tests were machined. Before final machining they were heat treated by solution annealing at 1200 °C for one hour followed by cooling in the air. The gauge length was mechanically and electrolytically polished.

### *2.2. Mechanical Testing*

Thermomechanical tests were performed using standard servohydraulic testing machine with hydraulic grips and high frequency inductive heating device in the temperature range of 250 to 700 °C. Cooling of the specimen was achieved by water cooled clamping jaws. Triangular wave form was used for mechanical and thermal cycling. Three types of loading were applied to the specimen, namely isothermal cyclic loading and in-phase and out of-phase TMF tests (IP-TMF and OP-TMF tests).

### *2.3. Initiation and the crack growth*

The surface relief of TMF cycled specimens was documented using Tescan Lyra3 XMU FESEM equipped with focused ion beam (FIB). The profiles of secondary cracks were revealed by producing FIB trenches. In order to study the crack paths the longitudinal sections parallel to the specimen axis of fatigued specimens were prepared. The relation of the grain boundary and crack paths was studied using electron back scatter diffraction (EBSD) technique.

## 3. Results

### *3.1. Mechanical Testing*

Cyclic hardening/softening curves along with the evolution of the mean stress during symmetric IP- and OP-TMF testing for four strain amplitudes are shown in Fig. 1. Cyclic hardening is characteristic for both types of TMF loading. The mean stress becomes positive in OP-TMF cycling and negative in IP-TMF cycling. The premature fracture prevents reaching the saturation of the stress amplitude during IP-TMF loading. In case of OP-TMF loading pronounced saturation is reached for all strain amplitudes.

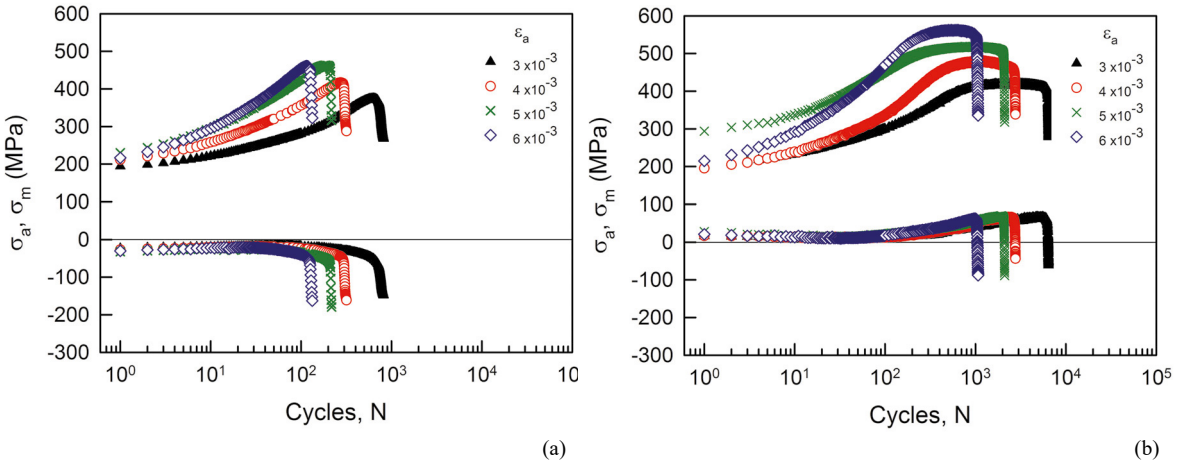


Fig. 1. Stress amplitude and mean stress in thermomechanical loading in the temperature range 250 °C to 700 °C; (a) IP-TMF; (b) OP-TMF.

Cyclic hardening/softening curves for various strain amplitudes during isothermal fatigue test conducted at 700 °C are shown in Fig. 2. Cyclic hardening during most of the fatigue life and the tendency to saturation for the lowest strain amplitudes are apparent.

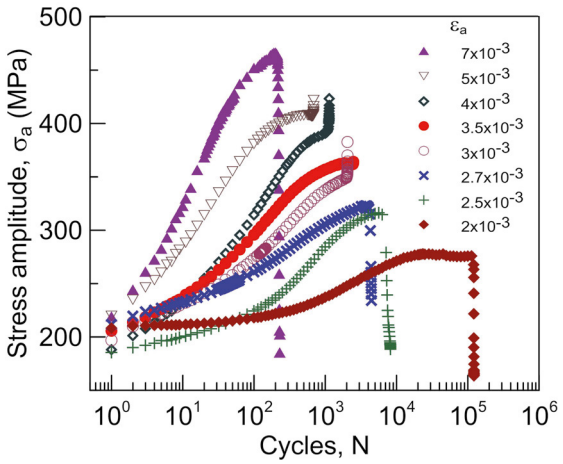


Fig. 2. Cyclic hardening/softening curves of Sanicro 25 steel in cyclic straining at temperature 700 °C.

Manson-Coffin fatigue life curves found for two types of TMF loading are shown in Fig. 3. For comparison isothermal Manson-Coffin curve at 700°C (fitted curve) is also plotted, Polák et al. (2014). Three specimens having approximately equal saturated plastic strain amplitudes were chosen for further study of damage mechanism.

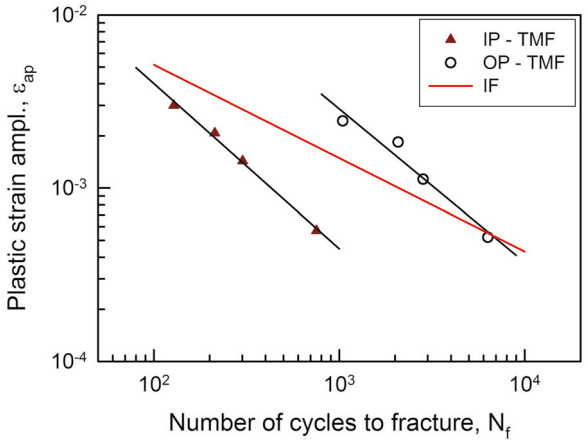


Fig. 3. Manson-Coffin fatigue life curve measured in three types of cyclic loading.

### *3.2. Surface relief*

TMF loading leads to the initiation of multiple fatigue cracks. It is the result of synergic effect of the varying temperature and strain as well as corrosion environment. In order to study the damage mechanism the secondary cracks in cracked specimens were observed in SEM. Damage evolution during TMF cyclic developed differently for IP-TMF and OP-TMF loading. The typical cracked surface of specimens cycled with mechanical strain amplitude $3x10^{-3}$ for both types of loading at the end of the fatigue life is shown in Fig. 4. The specimen surface after IP-TMF loading is covered by a thin oxide layer. Thicker oxide bands on some grain boundaries can be detected. The detail shown in Fig. 4a witnesses the crack development at the grain boundaries. Transgranular cracks running on the surface approximately perpendicular to the loading axis are typical for OP-TMF (Fig. 4b). More homogeneous and thicker oxide layer (in comparison with IP-TMF loaded specimen) developed during the OP-TMF cycling.

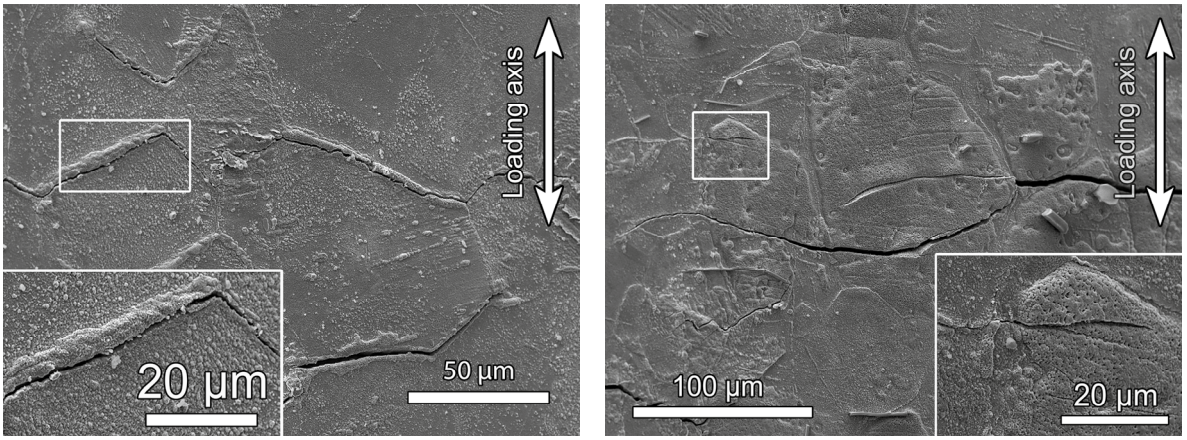


(a) (b)

Fig. 4. Surface of the specimen cyclically strained with mechanical strain amplitude $3x10^{-3}$ to fracture (a) IP-TMF cycling; (b) OP-TMF cycling.

Isothermal high temperature cyclic loading leads also to the formation of the inhomogeneous oxide layer on the material surface. Fig. 5 shows the bands of thicker oxide layer at the grain boundaries in the specimen cyclically strained with mechanical strain amplitude $3.5x10^{-3}$ for 250 cycles (10% $N_f$) at 700 °C. Grain boundaries are

preferentially oxidized. Since the specimen was subjected only to 250 cycles, pronounced and well developed cracks haven not been found. The inset in Fig. 5 shows early initiation of the crack at the grain boundary.

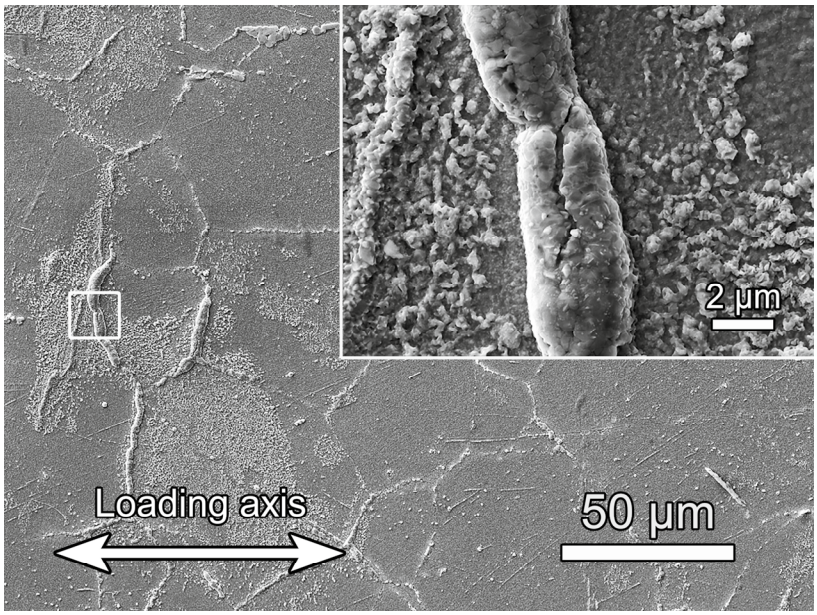


Fig. 5. Surface fatigue damage in Sanicro 25 steel cyclically strained with total strain amplitude $3.5x10^{-3}$for 250 cycles (10 % $N_f$) at temperature 700 °C.

### *3.3. FIB cuts*

The surface observations of specimens subjected to TMF loading indicate that in in-phase type of loading fatigue cracks develop at the grain boundaries by preferred oxidation. In order to see the crack development in 3D the FIB cut has been produced in location of the crack. Fig. 6a reveals the oxidation and cracking of the grain boundary perpendicular to the stress axis. The oxide/metal boundary is marked by the dotted line. The cracking of the grain boundaries in the early stages of the fatigue life leads to early macrocrack initiation and its rapid growth during the tensile part of the cycle at the increasing temperature.

Different mechanism of the fatigue crack initiation has been observed during OP-TMF loading. Thicker homogeneous oxide layer was formed and the grain boundaries were not attacked. OP-TMF cyclic loading leads to the formation of the transgranular cracks on the surface. Fig. 6 shows the FIB cut at one of the perpendicular cracks. The crack grows perpendicularly to the stress axis and closer inspection of the perpendicular cut reveals the oxide in the neighborhood of the crack. The oxide/metal interface is marked by the dotted line.

In isothermal high temperature cyclic loading the damage evolution was close to the in IP-TMF loading. Fig. 6c shows oxidized and cracked grain boundary revealed by FIB cut in the early stages of fatigue life (10% $N_f$).

### *3.4. The crack paths*

In order to study the crack propagation under two basic types of TMF loading longitudinal cuts of the cracked specimens were investigated using EBSD technique. The longitudinal cuts were produced from the gauge length of the tested specimens parallel to the loading axis. The secondary electron image and EBSD images of the cracks in IP- and OP-TMF loading have been obtained. Fig. 7 shows the crack produced in IP-TMF loading. The EBSD image confirms that crack path follows the grain boundaries. In the case of OP-TMF cycling, the transgranular crack propagation is evident, see Fig. 8.

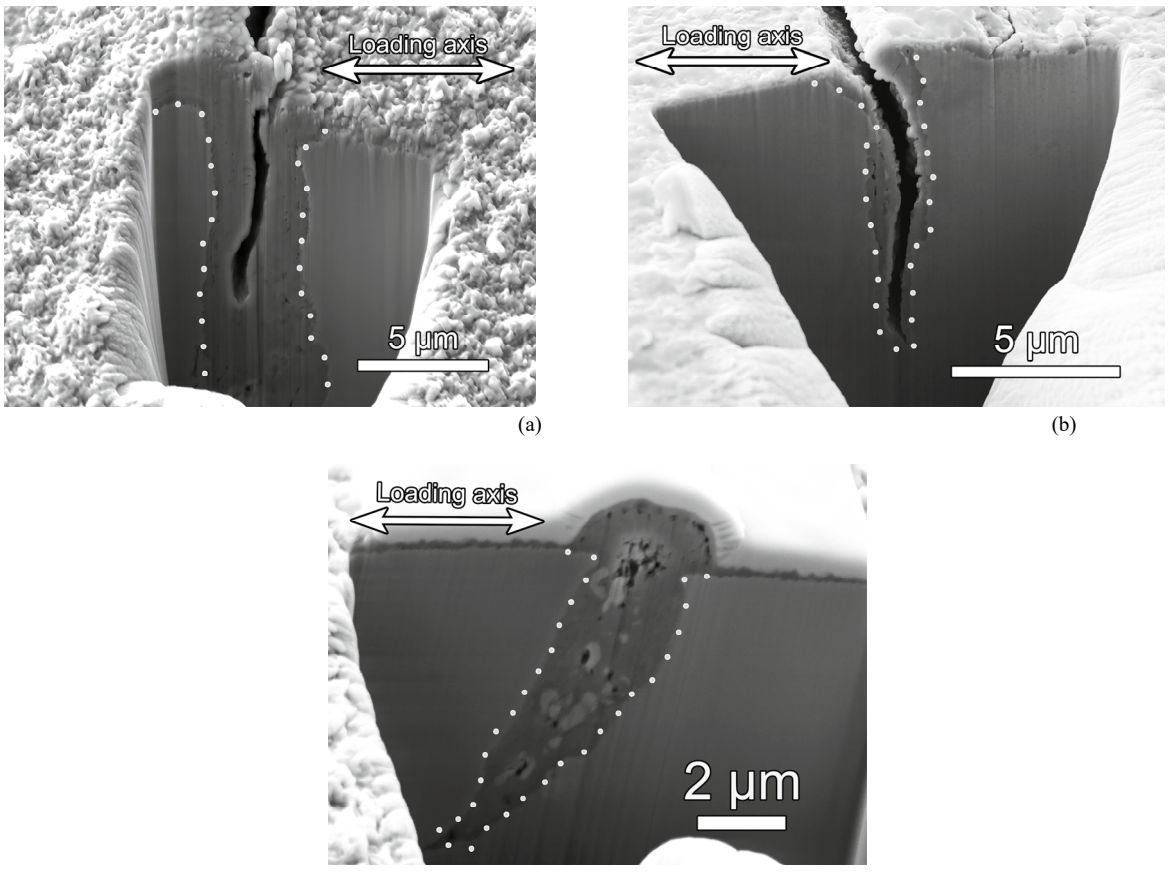


Fig. 6. FIB cut perpendicular to the surface; (a) cracked and oxidized grain boundary in a IP-TMF specimen; (b) transgranular surface crack with oxide close to the fracture surface (surface is in both cases covered by platinum layer); (c) Starting oxidation and cracking of the grain boundary in high temperature isothermal cyclic loading.

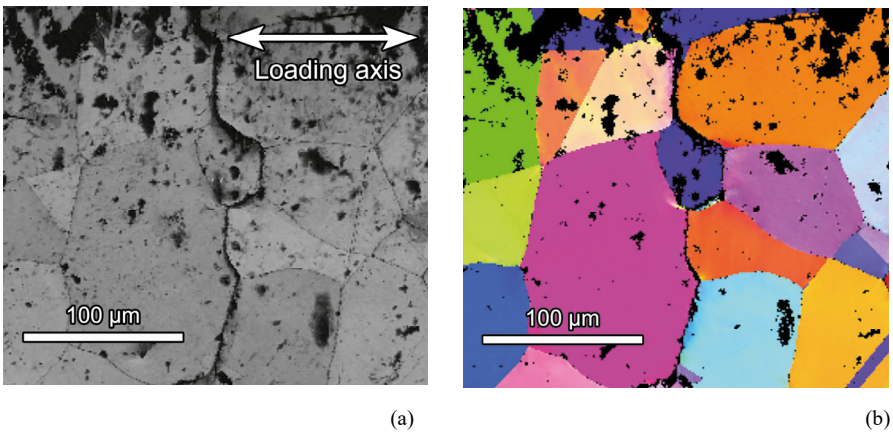


Fig. 7. Longitudinal section of the specimen subjected to IP-TMF cycling; (a) SEM image; (b) EBSD image.

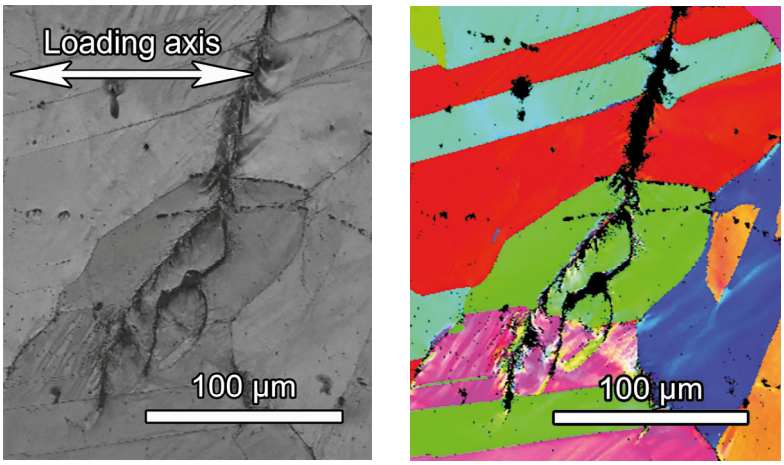


Fig. 8. Longitudinal section of the specimen subjected to OP-TMF cycling; (a) SEM image; (b) EBSD image.

## 4. Discussion

The investigation of the damage evolution under thermomechanical loading conditions of new heat resistant austenitic steel Sanicro 25 in the temperature range from 250 °C to 700 °C with constant mechanical strain amplitudes revealed substantially different damage mechanism in IP- and OP-TMF loading conditions.

The detailed investigation of the secondary cracks developed in the oxide layer allowed to understand the nature of the early crack initiation. During IP-TMF cycling fatigue cracks start in grain boundaries by preferred oxidation and cracking of the oxide (Fig.6a). The grain boundaries are preferentially exposed to oxidation while specimen is in tensile part of the cycle at high temperature. After intensive oxidation the oxide is cracked in compression at the bottom temperature of the cycle or during tensile loading at increasing temperature. This leads to intergranular crack initiation and propagation. The intergranular crack path was proved using EBSD technique (Fig. 7). Similar crack initiation mechanism was observed in Sanicro 25 steel during isothermal loading at 700 °C, Polák et al. (2014). The significant intergranular cracking in IP-TMF type of loading in temperature range 300-600 °C was also reported by Kuwabara and Nitta (1979). Different type of damage of AISI 316L SS during IP-TMF loading has been documented by Škorík et al. (2015). Mixed transgranular and intergranular cracking mode was observed in the temperature range 200-600 °C. However, the differences of the damage evolution for these two steels can be explained. Zauter et al. (1994) discussed the effect of the maximum temperature of the cycle on the lifetime and cracking mode as well. In cycling within the temperature intervals below the creep regime transgranular crack initiation and propagation prevails. The results indicate that fatigue, creep and environmental effects are the main damage contributions.

The cracks developed differently during OP-TMF type of loading. First of all the sufficient oxide layer on the specimen surface has to be formed. The oxide layer develops only at high temperature when specimen is in compression. The oxide layer becomes brittle at the lowest temperature in tensile part of the cycle which leads to random cracking of the oxide. The localized repeated oxidation and oxide cracking lead to transgranular crack growth (see Fig. 6b and Fig. 8). Nitta and Kuwabara (1988) classified the TMF life behavior according to the predominant damage mode. Since no contribution of creep is assumed for OP-TMF cycling, the environmental effects are decisive. They may lead to an embrittlement of the oxidized surface and give rise to an early crack initiation when high tensile loads coincide with low temperatures. Consequently, fatigue life under OP-TMF conditions may be reduced in comparison to IP-TMF cycling. According to our investigation rapid oxidation of grain boundaries in IP-TMF leads to high growth rate of fatigue cracks. Since the oxide layer during OP-TMF loading has to be thick enough to be cracked, crack initiation is delayed. The low oxidation rate of the cracks is due to the closure of the cracks in compression at high temperature. This lead to a slow crack growth and fatigue life during OP-TMF loading is thus prolonged (Fig. 3).

## 5. Conclusions

Experimental study of the Sanicro 25 under thermomechanical fatigue loading conditions lead to the following conclusions:

The effect of environment plays decisive role in damage evolution under TMF loading conditions provided the upper temperature of the TMF cycle is high.

The rapid oxidation of the grain boundaries during IP-TMF leads to the early cracking of the grain boundaries and propagation of the crack into volume of the material in intergranular manner. Similar damage mechanism is effective in isothermal cyclic straining at 700 °C.

In OP-TMF straining the homogeneous oxide layer is formed while the specimen is in compression. The delayed cracking of the oxide leads to development of cracks perpendicular to the loading axis. The localized repeated oxidation and cracking of the oxide results in transgranular crack growth.

The knowledge of the relevant damage mechanisms allows understanding differences in fatigue lives in IP- and OP-TMF cycling.

## Acknowledgement

The present work was conducted in the frame of IPMinfra supported through project No. LM2015069 and the project CEITEC 2020 No. LQ1601 of MEYS. The support by the project RVO: 68081723 and grant 13-23652S of GACR is gratefully acknowledged.

## References

Reddy, P.J., 2013. Clean coal technologies for power generation. CRCPress/Balkema, EH Leiden, The Netherlands.

Chai, G., Boström, M., Olaison, M., Forsberg, U., 2013. Creep and LCF Behaviors of Newly Developed Advanced Heat Resistant Austenitic Stainless Steel for A-USC. Procedia Engineering 55, 232 – 239.

Kuwabara, K., Nitta, A., 1979. Thermal–mechanical low cycle fatigue under creep– fatigue interaction on type 304 stainless steel. Procedia ICM 3, 69–78.

Kuwabara, K., Nitta, A., 1976. Effect of Strain Hold Time of High Temperature on Thermal Fatigue of Type 304 Stainless Steel. ASME-MPC symposium on creep– fatigue interaction. American Society of Mechanical Engineers, 161–77.

Zauter, R., Christ, H.-J., Mughrabi, H., 1994. Some Aspects of Thermomechanical Fatigue of AISI 304L Stainless Steel: Part I. Creep-Fatigue Damage. Metallurgical and Material Transactions 25A, 401- 406.

Nitta, A., Kuwabara, K., 1988. Thermal-Mechanical Fatigue Failure and Life Prediciton. Current Japanese Materials Research 3, 203–222.

Shi, H.J., Wang, Z.G., Su H.H., 1996. Thermomechanical Fatigue of a 316L Austenitic Steel at Two Different Temperature Intervals. Scripta Materialia 35(9), 1107–1113.

Hormozi, R., Biglari, F., Nikbin, K., 2015. Experimental Study of Type 316 Stainless Steel Failure under LCF/TMF Loading Conditions. International Journal of Fatigue 75, 153–169.

Polák, J., Petráš, R., Heczko, M., Kuběna, I., Kruml, T., Chai, G., 2014. Low Cycle Fatigue Behavior of Sanicro25 Steel at Room and at Elevated Temperature. Materials Science & Engineering A 615, 175–182.

Petráš, R., Škorík, V., Polák, J., 2016. Thermomechanical Fatigue and Damage Mechanisms in Sanicro 25 Steel. Materials Science & Engineering A 650, 52-62.

Škorík, V., Šulák, I., Obrtlík, K., Polák, J., 2015. Thermo-mechanical and Isothermal Fatigue Behavior of Austenitic Stainless Steel AISI 316L, Metal Conference Proceedings, 85.